

Article

Microstructure and Corrosion Characterization of Cr Film on Carburized CSS-42L Aerospace Bearing Steel by Filtered Cathodic Vacuum Arc Deposition

Fangfang Wang ^{1,2}, Qiushi Li ^{2,*}, Lijing Zheng ¹, Fengxiang Zhang ¹ and Hu Zhang ^{1,*}

¹ School of Materials Science and Engineering, Beihang University, Beijing 100191, China; wangfangfang@buaa.edu.cn (F.W.); zhenglijing@buaa.edu.cn (L.Z.); zhangfengxiang@buaa.edu.cn (F.Z.)

² School of Energy and Power Engineering, Beihang University, Beijing 100191, China

* Correspondence: liqs@buaa.edu.cn (Q.L.); zhanghu@buaa.edu.cn (H.Z.);
Tel.: +86-10-8233-9651 (Q.L.); +86-10-8231-6958 (H.Z.)

Received: 18 July 2018; Accepted: 3 September 2018; Published: 6 September 2018



Abstract: For present and future advanced aerospace bearing applications, it is significant and necessary to improve the corrosion resistance of carburized CSS-42L steel. In this study, Cr films of about 1 μm in thickness were fabricated onto carburized CSS-42L bearing steel using a filtered cathodic vacuum arc deposition system. The corrosion behavior of carburized CSS-42L steel with Cr films was investigated. The Cr film was composed of nanocrystalline α -Cr. The electrochemical experimental results indicated that the current density had two orders of magnitude decrease and the corrosion potential evidently increased after Cr film deposition. The protective efficiency of this Cr film was as high as 99.7%. Nanocrystalline exhibits a higher corrosion resistance and enhances the modification effect of Cr film on carburized CSS-42L steel.

Keywords: CSS-42L bearing steel; filtered cathodic vacuum arc; nanocrystalline Cr film; corrosion behavior

1. Introduction

Aircraft engines are one of the most sophisticated engineering technologies [1]. The impact of the gas turbine engine on the development of the aircraft industry creates urgent requirements for better materials and designs for bearings. They need to tolerate increased system temperature, speed and load capability [1–4]. The analysis of engine field failures has shown that the classical material fatigue failure initiated on the subsurface has nearly disappeared. Instead, the dominant bearing failures are caused by surface-initiated fatigue resulting from contaminants such as corrosion pit [4–6]. Next generation main shaft bearings for future advanced gas turbine engines should operate under conditions of extreme temperature, high loads and harsh, corrosive environments [7]. M50 and M50NiL alloys are frequently used for medium-temperature aerospace main shaft bearing steels. M50 provides good wear resistance but is poor in terms of both fracture toughness and corrosion resistance. M50NiL was developed as a low-carbon variant of M50, enriched with nickel for excellent fracture toughness, but is inadequate in terms of wear resistance and is also deficient in terms of corrosion resistance [1,7–10]. The increasing demands for alloys combining all these characteristics have led to the development of case-hardened high-temperature CSS-42L steel. It defines a case-core structure and has two sets of properties. The carburized surface has higher hardness, rolling contact fatigue resistance, wear resistance and relatively better corrosion resistance. The specific core provides adequate fracture toughness and strength [11]. The optimized heat treatment of CSS-42L steel meets most of the aerospace bearing requirements. However, its corrosion resistance after carburizing greater than AISI 440C has not yet been achieved [7,9].

Surface modification is a useful way to improve the corrosion resistance of bearings for aerospace applications. Various surface treatment techniques such as ion implantation, laser shock peening and coating deposition have been used to modify the corrosion property of bearing steels. It was reported that DLC, or “metallic ceramics”, such as TiN, CrN, TiC, CrC, etc., on stainless steel or other substrates made them promising corrosion-resistant coating materials [12–15]. As is known, the continuous protective Cr_2O_3 formed between the base metal and the environment (oil, water, air, etc.) creates the stainless behavior. There has also been a great deal of research into Cr ion implantation or Cr film deposition to improve the corrosion resistance of treated matrix materials [6,16,17]. Pearson et al. [6] pointed out that the thin dense chromium film can improve the life of M50NiL under contamination conditions.

Electroplating is a widely used method in industry. Traditionally used hexavalent chromium electrolytes have been shown to be toxic and carcinogenic and this process is strictly restricted now. Trivalent chromium plating is considered to be the most attractive alternative due to its eco-friendly properties [18–21]. However, the process of metallic chromium electrodeposition from trivalent chromium electrolytes is complicated. In addition, the deposited coatings are mainly amorphous and rarely pure chromium coatings, which present obvious flaws, such as high brittleness, low hardness and a poor bonding force. Thus far, the trivalent chromium plating process has not reached industry development [18,19,21]. The filtered cathodic vacuum arc technique (FCVA) is a deposition system that is appreciated both in industrial applications and in innovative research. Various single element films including metals, silicon, carbon, many ceramics coatings and semiconductor films have been deposited using this method [22,23]. It was confirmed that FCVA deposition is a promising technique for the production of high-quality films, achieved through the nano-structure, increased strength of adhesion and packing density of coating to substrate, and reduced coating surface defects [22,24]. However, to our best knowledge, little work has been reported on chromium film deposition on high-temperature bearing steel CSS-42L using the FCVA process.

In the present study, we investigated the fabrication of Cr films on carburized CSS-42L steel substrate using the FCVA deposition system. The film microstructure, surface morphology and corrosion properties of Cr films deposited on carburized CSS-42L steel were assessed with a wide range of characteristic techniques.

2. Materials and Methods

2.1. Substrate Materials and Film Synthesis

The experiment CSS-42L steel was prepared using vacuum induction melting and a casting furnace, before undergoing a forging and annealing treatment. Its nominal composition (wt %) is 13.73 Cr, 13.0 Co, 4.6 Mo, 2.11 Ni, 0.6 V, 0.33 Mn, 0.2 Si, 0.024 Nb, 0.002 B, 0.14 C and balance Fe. The CSS-42L was carburized in an atmosphere furnace and subsequently hardened. The hardening treatment consisted of the following steps:

- Austenitizing at 1095 °C for 15 min;
- Quenching in oil down to room temperature;
- Deep cryogenic treatment for 5 h;
- Tempering at 495 °C for 2 h;
- Deep cryogenic treatment for 5 h;
- Tempering at 495 °C for 2 h.

Specimens of $10 \times 10 \times 5 \text{ mm}^3$ were mechanically polished with SiC emery papers up to #2000, and polished, finally, with diamond paste to 1.5 μm grit. Before the ion implantation and deposition, the samples were ultrasonically degreased in acetone. All the depositions were made using a FCVA deposition machine (Beijing Normal University, Beijing, China). The arc cathode was a high-purity chromium rod. In order to improve the adhesion of the deposited coating, the samples were sputter-etched with Cr ions prior to each experiment in the vacuum chamber, and then continuously

implanted with Cr ions to a dose of 1×10^{17} ions/cm² at an energy of 8 keV. Finally, thin chromium films with a thickness of ~ 1 μm were deposited on the pretreated samples. During the deposition process, a pulse arc current of 100 A and a dc pulsed a negative bias of -80 V with a duty cycle of 90% in a 180°-bend magnetic FCVA system were normally applied. For convenience, the specimens discussed in this paper may be referred to using an abbreviation based on their processing source. After carburizing, the CSS-42L steel was abbreviated to (C + C). The carburized CSS-42L with chromium deposition was abbreviated to (C + C)–Cr.

2.2. Characterization of the Deposited Cr Film

The surface topography was measured using an atomic force microscopy (ICON AFM, Veeco/Bruker, Santa Barbara, CA, USA) and NanoScope Analysis software (NanoScope Analysis 1.40) was used to calculate the arithmetic mean roughness (R_a). The longitudinal section microstructure of the film was observed using a scanning electronic microscopy (SEM, CamScan-3400, Cambridge, UK) and its composition was detected using Energy Disperse Spectroscopy (EDS). The crystallographic phases were determined by X-ray diffraction (XRD, Rigaku, Tokyo, Japan) with a Cu K α source at 0.154 nm and the glancing angle X-ray diffraction (GAXRD, Bruker AXS, Karlsruhe, Germany) at 0.5° was used to discern the phases in the Cr film. The cross-section view of the thin film was observed using transmission electron microscopy (JEOL TEM 2100, 200 kV, Tokyo, Japan).

2.3. Corrosion Behavior Measurements

Polarization studies were performed in a 3.5% NaCl solution to investigate the electrochemical corrosion behavior of the carburized CSS-42L and the Cr-coated specimens. Potentiodynamic polarization scans were carried out using a CS300 electrochemical work station (Corrtest, Wuhan, China). The NaCl solution was maintained at 30 °C open to air and the potentiodynamic curves were initiated once the open circuit potential was stabilized. For the study, a conventional three-electrode cell system was used, in which a platinum sheet and a saturated calomel electrode (SCE, Ruosull Technology Ltd., Shanghai, China) were used as the counter and reference electrode, respectively. The scanning rate was 0.5 mV/s.

The surface chemistry of the carburized CSS-42L and Cr film-coated samples after the polarization study was determined using X-ray photo electron spectroscopy (XPS, ULVAC-PHI, Kanagawa, Japan). All the XPS results were attained at a depth of 3 nm from the outmost surface. The corrosion morphology was examined using SEM and the composition of the corrosion products was analyzed using SEM/EDS.

3. Results and Discussion

3.1. Surface and Cross-Sectional Morphology

In Figure 1a, cross-sectional SEM images of (C + C)–Cr are shown. The Cr film has a compact and homogeneous layer adhered to the substrate and its average thickness is about 1.1 μm . The composition line scanning result of the coating is presented in Figure 1b. The width of the Cr enrich zone is nearly equivalent to that observed in Figure 1a. The line analysis also reveals that the Cr concentration is highest near the surface and gradually decreases. There is no abrupt drop in Cr content at the boundary between the Cr rich layer and the substrate. The chromium ion implantation layer before the Cr film deposition may be responsible for this composition transition and have the benefit of increasing the adhesion between the coating and the substrate.

The corrosion properties of the coatings relate to the surface density and roughness. The surface morphology of the Cr film was investigated using an AFM. Figure 2 demonstrates 2D and 3D images in a 1×1 μm^2 square of the deposited film. The measured arithmetic means of R_a of (C + C) and (C + C)–Cr are given as 1.01 nm and 3.95 nm, respectively. The Cr coating consisted of spherical-like particles with sizes of 80–100 nm. The increase in coating roughness may be correlated with its trend

to grow in a columnar structure [25]. The surface topography of the Cr film shows an almost uniform and dense structure.

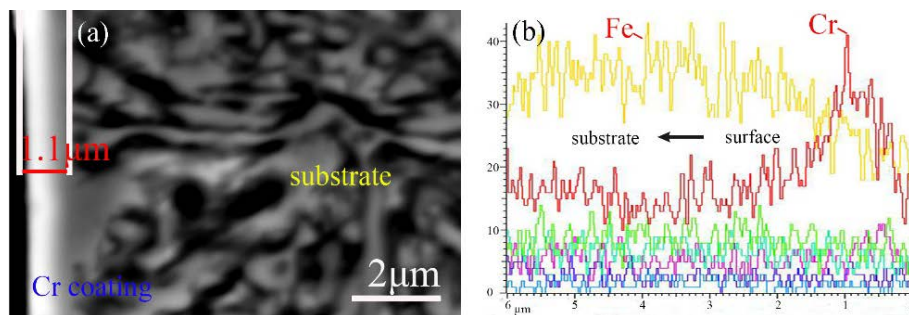


Figure 1. SEM image of transverse of Cr coating deposited using the FCVA system (a) and the line analysis of the compositional element distribution along the substrate to the outmost layer (b).

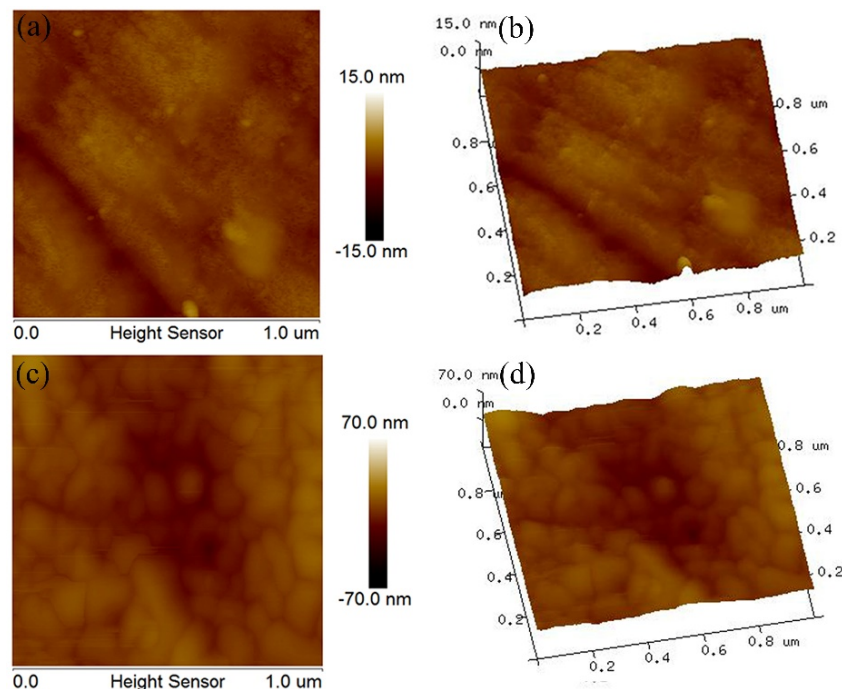


Figure 2. AFM 2D and 3D images in a $1 \times 1 \mu\text{m}^2$ square of the substrate samples (a,b) and Cr film-coated samples (c,d), respectively

3.2. Structural Information

Figure 3 presents the XRD patterns for the (C + C)–Cr specimen. The diffraction peaks corresponding to the (110) and (211) indexed values of α -Cr were detected. GAXRD at 0.5° was conducted to investigate the phase constituents on the subsurface of Cr film where no oxide peaks appear. The position of the (211) diffraction peak and the full width of the peak at half maximum were used to estimate the mean grain size of the coating using the Debye-Scherrer equation [26,27]:

$$D = \frac{0.9\lambda}{B \cos \theta} \quad (1)$$

where D is the average dimension of crystalline, B is the full width at half maximum (FWHM), λ is the wavelength of the X-ray radiation and θ denotes the Bragg diffraction angle. The calculated

average grain diameter in the Cr film was about 90 nm, which was close to that determined using AFM measurements.

TEM observation was performed to investigate the more detailed microstructure of the deposited Cr film. Figure 4a,b shows the bright-field micrograph and the center dark-field micrograph of the Cr film, respectively. The deposited Cr film has a microstructure with crystal grain of fine and homogeneous. The TEM-EDS results and the selected area electron diffraction (SAED) pattern of the Cr coating are presented separately in Figure 4c,d. The corresponding SAED pattern includes discontinuous diffraction rings of α -Cr, indicating that the deposited films consist of nanometer polycrystalline α -Cr. Former research found that a nanocrystalline coating with a homogenous microstructure could promote the corrosion resistance of metals/alloys [28–30].

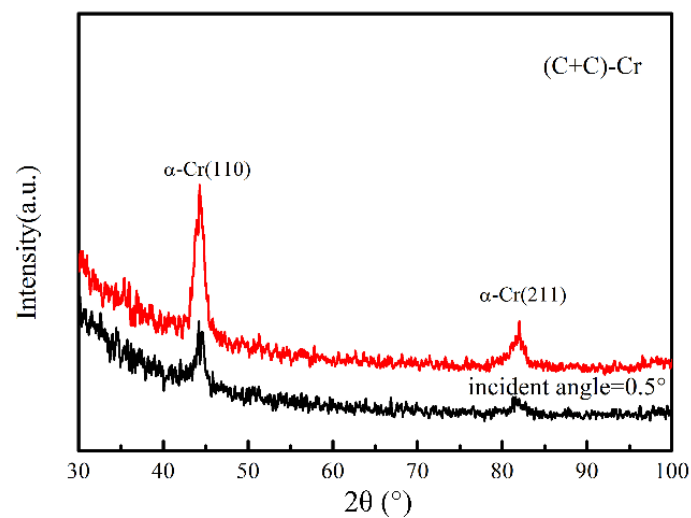


Figure 3. Normal XRD pattern and GAXRD diffractogram at a grazing angle of 0.5° in the 30° – 100° diffraction angles region for the carburized CSS-42L samples with Cr deposition ((C + C)–Cr).

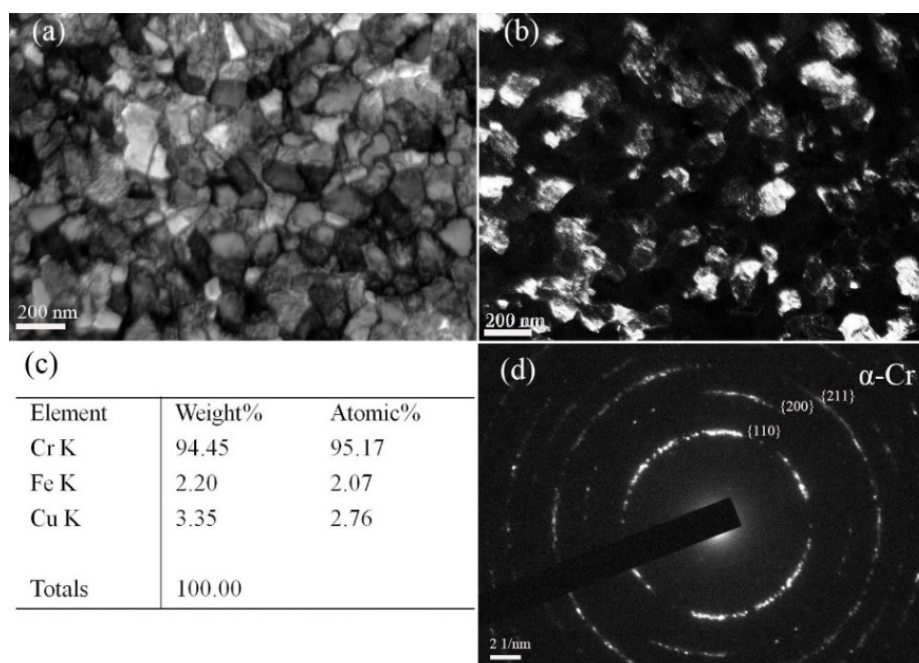


Figure 4. (a,b) TEM bright and dark images of Cr film and (c,d) corresponding TEM-EDS results and electron diffraction pattern, respectively.

3.3. Potentiodynamic Polarization Test

Figure 5 depicts the potentiodynamic polarization curves for the carburized CSS-42L steel samples with and without Cr films in a 3.5% NaCl solution. For carburized CSS-42L steel, the corrosion potential value was about -0.42 V and the corrosion current density was about 9.8×10^{-6} A cm $^{-2}$. There was no passivation region; instead, the corresponding corrosion current density was quite high and the current density raised at a high rate immediately after the corrosion potential under the testing conditions. Generally, a rapid increase in current density resulted from the breakdown of the passive film, and is always accompanied by localized corrosion [31]. However, for the Cr deposited sample, the corrosion potential was greatly increased to -0.12 V and the corrosion current density was approximately 3.0×10^{-8} A cm $^{-2}$. In addition, the Cr deposited specimen had a passivation region where the current density increased slowly with the potential increase. The anodic current density of the Cr deposited sample was over two orders of magnitude lower than that of an uncoated sample, suggesting that the corrosion rate of the Cr deposited sample was far less than that of the uncoated one. At higher potentials, the transpassivity branch was observed as indicated by the sudden increase in current density. Pitting also occurred for the Cr deposited samples. However, the pitting potential, which has a value of about 0.3 V for the Cr deposited specimen, was much higher than -0.4 V for the untreated steel.

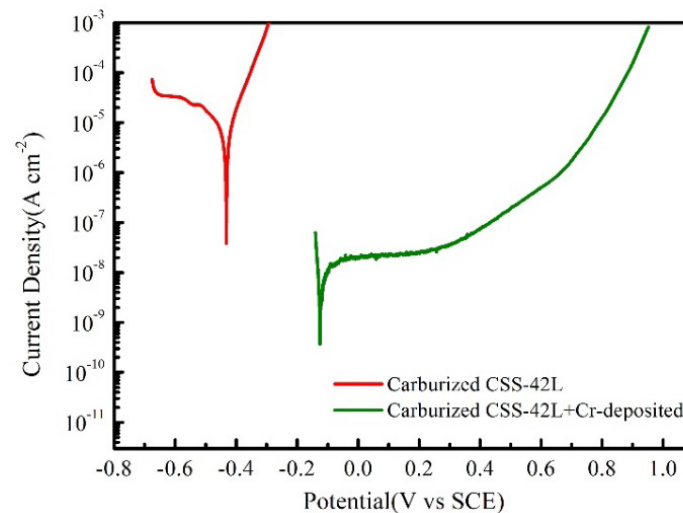


Figure 5. Potentiodynamic polarization plots of the carburized CSS-42L sample with and without Cr film deposition.

The higher corrosion potential, lower anodic current density and higher pitting potential of the Cr-coated specimens show that the corrosion resistance of the carburized CSS-42L steel was improved by the Cr deposition treatment. The protective efficiency (P_e) of the deposited Cr film was evaluated using the following equation [32–34]:

$$P_e(\%) = \left(\frac{i_{corr}^0 - i_{corr}}{i_{corr}^0} \right) \times 100\% \quad (2)$$

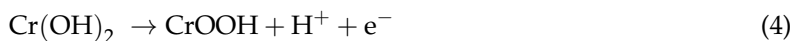
where i_{corr}^0 and i_{corr} refer to the corrosion current densities in the absence and presence of a Cr coating layer, respectively. The P_e value of the deposited Cr film was 99.7%. This result supports the conclusion that Cr film deposition using the FCVA technique is an effective means to improve the corrosion resistance of carburized CSS-42L steel.

It is known that the formation of a protective oxide film in which chromium is the main cation is responsible for the good corrosion resistance of stainless steels. The study of the electrochemical and passivation properties of pure chromium reveals its anodic dissolution proceeds and the passivation

reaction. The anodic dissolution behavior is the oxidation of chromium metal to Cr^{2+} . The formation of Cr^{3+} -oxygen species on the corroding surface is related to the passivation process. Björnkvist et al. [35] proposed that a layer of $\text{Cr}(\text{OH})_2$ was formed on the actively corroding surface. Thus, the anodic dissolution process being:



the passivation mechanism is proposed as follows:



The dissolution and passivation reactions proceed in parallel. The content of intermediate $\text{Cr}(\text{OH})_2$ and the stability of CrOOH contributed to corrosion resistance of the chromium film. In the present study, the grain size of the chromium coating was nanometer, which could improve the Cr diffusion further and form a more compact passive film. Similar results have been found for Ni-based alloys or stainless steels with a nanocrystalline coating [29,30,36].

Generally, chloride ion is the most aggressive anion resulting in localized corrosion on stainless steels or other metals. On the one hand, chloride ions may react with the intermediate $\text{Cr}(\text{OH})_2$, which decreases its coverage on the corroded surface. Previous reports have shown that the smaller grain size is more beneficial for decreasing the content of Cl^- absorption on the surface [30,36]. Compared with the electrochemical results of conventional electroplated chromium film, which is composed of micrometer grains [37,38], the nanocrystalline chromium film in the present work had more positive corrosion potential, which has a reverse correlation with the absorption of Cl^- .

Above all, the experimental Cr film deposited using the FCVA technique composed of nanometer grains, and the refining of the grain size, was beneficial for the formation of more compact passive film, which significantly enhanced the corrosion resistance of carburized CSS-42L steel.

3.4. Characterization of the Passive Film and Corrosion Morphology

The potentiodynamic polarization curves showed that the passive current density of the experimental samples was obviously different. The properties of passive film play an important role in influencing the magnitude of the current density [30]. An XPS analysis was conducted to provide more detailed information about the passive films formed in a 3.5% NaCl solution. The fitting results are shown in Figure 6. In the passive film of carburized CSS-42L steel (Figure 6b), the Fe2p, Cr2p and Mo3d peaks consisted of their metallic and oxide states. According to the peak strength, the main component in the passive film was Fe^{3+} in Fe_2O_3 at 710.7 eV, Fe^{2+} in FeO at 709 eV and Cr^{3+} in Cr_2O_3 at 575.6 eV. The CrO_x peaks at 576.6 and 577.7 eV are chromium native oxides which correspond to CrOOH or $\text{Cr}(\text{OH})_3$ [39]. In the Cr-coated sample (Figure 6a), the passive film was mainly composed of chromium oxides and hydroxides. Weak Fe2p and Mo3d peaks could also be detected in this passive film which might be diffused from the matrix material. It is generally accepted that the protectiveness of these films, which contained more chromium oxides and hydroxides, was higher. These XPS analysis results regarding the passive composition correspond well with the polarization measurements.

The surface morphology of the carburized CSS-42L samples after the corrosion test in a 3.5% NaCl solution with and without Cr film is demonstrated in Figure 7. The pictures clearly delineate the improvement in corrosion resistance for the Cr-coated sample. The SEM images obtained for the uncoated sample after the corrosion test showed a heavy attack (Figure 7b). The microstructure of the matrix was exposed and there were many pits distributing on the surface. Intergranular corrosion and crevice corrosion phenomena were also observed on the uncoated sample. Pitting corrosion was also detected in the chromium-coated sample and the size of the pitting holes was a little larger than that in the uncoated sample, which may be related to the degradation of the coating film (Figure 7a). However, the surface morphology preserved almost its original appearance and the number of pits decreased dramatically. The chemical composition of the corrosion products was also investigated using an SEM-EDS (shown in Table 1). Fe, Cr, Co, O and Cl were detected in the corrosion products.

For the chromium-coated sample, the Cl content was relatively lower. Cr₂O₃ is a p-type semiconductor with redundant cation which can reduce Cl⁻ ion adsorption [30].

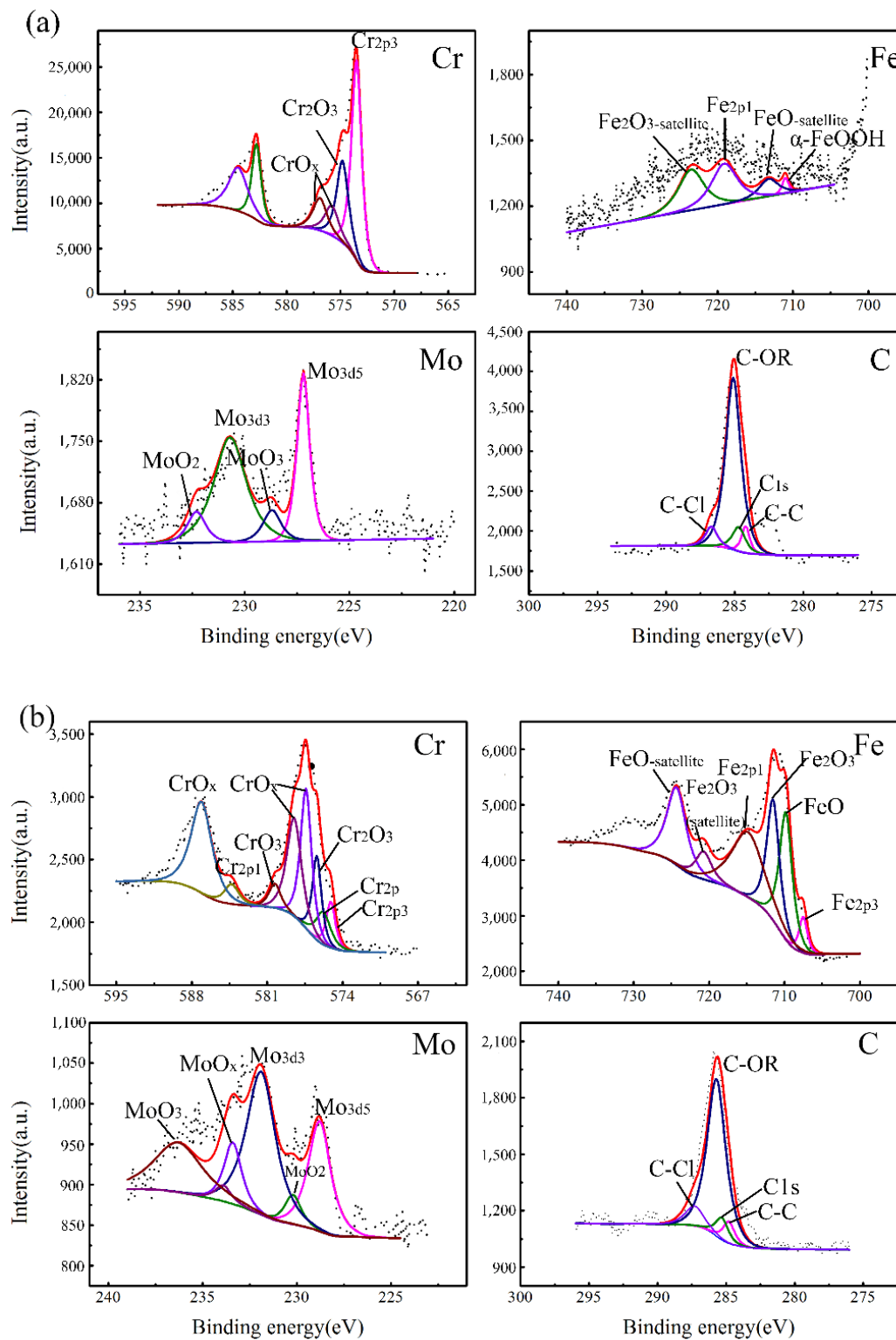


Figure 6. Cr_{2p}, Fe_{2p}, Mo_{3d} and C_{1s} XPS spectra from carburized CSS-42L specimens with chromium coating (a) and uncoated (b) after a polarization test in a 3.5% NaCl solution.

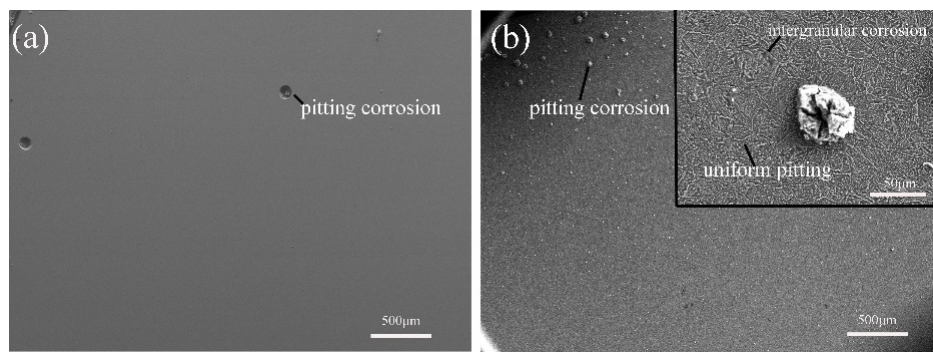


Figure 7. SEM micrographs of the corroded surface on carburized CSS-42L samples: (a) with Cr film deposition, (b) without Cr film deposition.

Table 1. Chemical composition of corrosion products detected using an SEM-EDS for carburized CSS-42L specimens with and without chromium coating.

Sample	Fe (at %)	Cr (at %)	Co (at %)	O (at %)	Cl (at %)
(C + C)	43.41	5.43	9.66	29.04	12.17
(C + C)–Cr	55.33	2.30	12.12	26.97	3.11

4. Conclusions

The structure, morphology and corrosion protection efficiency of Cr films deposited on carburized CSS-42L bearing steel using the FCVA technique have been investigated. Based on the above experimental results and discussion, the conclusions can be summarized as follows:

- SEM, AFM and TEM analyses have revealed that a uniform and dense Cr film with a homogeneous distribution of particles was introduced using the FCVA deposition system. The grain size of α -Cr was about 100 nm.
- The nanocrystalline Cr coating significantly improved the corrosion resistance of the carburized CSS-42L steel in a 3.5% NaCl solution. The Cr-coated samples had two orders of magnitude lower current densities and evidently increased corrosion potential. The protective efficiency of the deposited Cr film is as high as 99.7%. The passive film of the Cr-coated sample was mainly composed of Cr_2O_3 .
- Nanometer grains improve Cr diffusion and decrease the content of Cl^- absorption on the surface, which contributed to forming a more compact and protective passive film. The nanocrystalline further enhances the modification effect of chromium coating on carburized CSS-42L bearing steel.

Author Contributions: Conceptualization, F.W., Q.L., L.Z. and H.Z.; Investigation, F.W., F.Z.; Writing-Original Draft Preparation, F.W.; Writing-Review & Editing, F.W., Q.L. and H.Z.; Supervision, Q.L. and H.Z.

Funding: This research was funded by the China Postdoctoral Science Foundation (230210441).

Conflicts of Interest: The authors declare no conflicts of interest.

References

1. Bhadeshia, H.K.D.H. Steels for bearings. *Prog. Mater. Sci.* **2012**, *57*, 268–435. [[CrossRef](#)]
2. Zaretsky, E.V. Rolling bearing steels—A technical and historical perspective. *Mater. Sci. Technol.* **2012**, *28*, 58–69. [[CrossRef](#)]
3. Ooi, S.; Bhadeshia, H.K.D.H. Duplex hardening of steels for aeroengine bearings. *ISIJ Int.* **2012**, *52*, 1927–1934. [[CrossRef](#)]
4. Streit, E.; Brock, J.; Poulin, P. Performance evaluation of “duplex hardened” bearings for advanced turbine engine applications. *J. ASTM Int.* **2006**, *3*, 1–9. [[CrossRef](#)]

5. Ebert, F.J. An overview of performance characteristics, experiences and trends of aerospace engine bearings technologies. *Chin. J. Aeronaut.* **2007**, *20*, 378–384. [[CrossRef](#)]
6. Pearson, P.K. The history and future of aircraft turbine engine bearing steels. In *Bearing Steels: Into the 21st Century*; Hoo, J.J.C., Green, W.B., Eds.; ASTM International: West Conshohocken, PA, USA, 1998; Volume 1327, pp. 335–353.
7. Burrier, H.I.; Tomasello, C.M.; Balliett, S.A.; Maloney, J.L.; Milam, D.L.; Ogden, W.P. Development of CSS-42L™, a high performance carburizing stainless steel for high temperature aerospace applications. In *Bearing Steels: Into the 21st Century*; Hoo, J.J.C., Green, W.B., Eds.; ASTM International: West Conshohocken, PA, USA, 1998; pp. 374–390.
8. Nygaard, J.R.; Rawson, M.; Danson, P.; Bhadeshia, H.K.D.H. Bearing steel microstructures after aircraft gas turbine engine service. *Mater. Sci. Technol.* **2014**, *30*, 1911–1918. [[CrossRef](#)]
9. Ragen, M.A.; Anthony, D.L.; Spitzer, R.F. A comparison of the mechanical and physical properties of contemporary and new alloys for aerospace bearing applications. In *Bearing Steels Technology*; Beswick, J.M., Ed.; ASTM International: West Conshohocken, PA, USA, 2002; pp. 362–374.
10. Bamberger, E.N.; Clark, J.C.; Nahm, A.H. Rolling Element Bearing Member. U.S. Patent 4,659,241, 21 April 1987.
11. Rai, A.K.; Bhattacharya, R.; Trivedi, H.K. Wear Resistant Coatings for Race Land Regions of Bearing Materials. U.S. Patent 7,910,217, 22 March 2011.
12. Zhang, M.; Wu, B.; Lin, G.; Shao, M.; Hou, M.; Yi, B. Arc ion plated Cr/CrN/Cr multilayers on 316L stainless steel as bipolar plates for polymer electrolyte membrane fuel cells. *J. Power Sources* **2011**, *196*, 3249–3254. [[CrossRef](#)]
13. Picraux, S.T.; Pope, L.E. Tailored surface modification by ion implantation and laser treatment. *Science* **1984**, *226*, 615–622. [[CrossRef](#)] [[PubMed](#)]
14. Zhang, H.; Lin, G.; Hou, M.; Hu, L.; Han, Z.; Fu, Y.; Shao, Z.; Yi, B. CrN/Cr multilayer coating on 316L stainless steel as bipolar plates for proton exchange membrane fuel cells. *J. Power Sources* **2012**, *198*, 176–181. [[CrossRef](#)]
15. Guan, X.; Wang, Y.; Xue, Q.; Wang, L. Toward high load bearing capacity and corrosion resistance Cr/Cr₂N nano-multilayer coatings against seawater attack. *Surf. Coat. Technol.* **2015**, *282*, 78–85. [[CrossRef](#)]
16. Zeng, Z.; Wang, L.; Chen, L.; Zhang, J. The correlation between the hardness and tribological behaviour of electroplated chromium coatings sliding against ceramic and steel counterparts. *Surf. Coat. Technol.* **2006**, *201*, 2282–2288. [[CrossRef](#)]
17. Podgoric, S.; Jones, B.J.; Bulpett, R.; Troisi, G.; Franks, J. Diamond-like carbon/epoxy low-friction coatings to replace electroplated chromium. *Wear* **2009**, *267*, 996–1001. [[CrossRef](#)]
18. Gedvidas, B.; Asta, Č.; Aušra, S.; Vidas, P.; Tadas, M. Dry sliding tribological behavior of Cr coatings electrodeposited in trivalent chromium sulphate baths. *Surf. Coat. Technol.* **2017**, *315*, 130–138.
19. Quan, C.; He, Y. Properties of nanocrystalline Cr coatings prepared by cathode plasma electrolytic deposition from trivalent chromium electrolyte. *Surf. Coat. Technol.* **2015**, *269*, 319–323. [[CrossRef](#)]
20. Liao, C.W.; Lee, H.B.; Hou, K.H.; Jian, S.; Lu, S.; Ger, M. Characterization of the Cr-C/Si₃N₄ composite coatings electroplated from a trivalent chromium bath. *Electrochim. Acta* **2016**, *209*, 244–253. [[CrossRef](#)]
21. Liang, A.; Qiao, L.; Zhang, B.; Ni, L.; Zhang, J. Preparation of crystalline chromium coating on Cu substrate directly by DC electrodeposition from wholly environmentally acceptable Cr(III) electrolyte. *Mater. Lett.* **2014**, *119*, 131–134. [[CrossRef](#)]
22. Paternoster, C.; Zhirkov, I.; Delplancke-Ogletree, M.P. Structural and mechanical characterization of nanostructured titanium oxide thin films deposited by filtered cathodic vacuum arc. *Surf. Coat. Technol.* **2013**, *227*, 42–47. [[CrossRef](#)]
23. Hee, A.C.; Zhao, Y.; Jamali, S.S.; Martin, P.J.; Bendavid, A.; Peng, H.; Cheng, X. Corrosion behaviour and microstructure of tantalum film on Ti6Al4V substrate by filtered cathodic vacuum arc deposition. *Thin Solid Films* **2017**, *636*, 54–62. [[CrossRef](#)]
24. Vereschaka, A.A.; Vereschaka, A.S.; Batako, A.D.; Mokritskii, B.J.; Aksenenko, A.Y.; Sitnikov, N.N. Improvement of structure and quality of nanoscale multilayered composite coatings, deposited by filtered cathodic vacuum arc deposition method. *Nanomater. Nanotechnol.* **2017**, *7*. [[CrossRef](#)]
25. Corbella, C.; Oncins, G.; Gomez, M.A. Structure of diamond-like carbon films containing transition metals deposited by reactive magnetron sputtering. *Diam. Relat. Mater.* **2005**, *14*, 1103–1107. [[CrossRef](#)]

26. Wang, N.; Zhou, C.; Gong, S.; Xu, H. Heat treatment of nanostructured thermal barrier coating. *Ceram. Int.* **2007**, *33*, 1075–1081. [[CrossRef](#)]
27. Shaw, L.L.; Goberman, D.; Ren, R.; Gell, M.; Jiang, M.; Wang, Y.; Xiao, T.D.; Strutt, P. The dependency of microstructure and properties of nanostructured coatings on plasma spray conditions. *Surf. Coat. Technol.* **2000**, *130*, 1–8. [[CrossRef](#)]
28. Zheng, Z.J.; Gao, Y.; Gui, Y.; Zhu, M. Corrosion behaviour of nanocrystalline 304 stainless steel prepared by equal channel angular pressing. *Corros. Sci.* **2012**, *54*, 60–67. [[CrossRef](#)]
29. Liu, L.; Li, Y.; Wang, F. Electrochemical corrosion behavior of nanocrystalline materials—A review. *J. Mater. Sci. Technol.* **2010**, *26*, 1–14. [[CrossRef](#)]
30. Liu, L.; Li, Y.; Wang, F. Influence of grain size on the corrosion behavior of a Ni-based superalloy nanocrystalline coating in NaCl acidic solution. *Electrochim. Acta* **2008**, *53*, 2453–2462. [[CrossRef](#)]
31. Li, C.X.; Bell, T. Corrosion properties of plasma nitrided AISI 410 martensitic stainless steel in 3.5% NaCl and 1% HCl aqueous solutions. *Corros. Sci.* **2006**, *48*, 2036–2049. [[CrossRef](#)]
32. Nam, N.D.; Han, J.H.; Kim, J.G.; Tai, P.H.; Yoon, D.H. Electrochemical properties of TiN/CrN-coated bipolar plates in polymer electrolyte membrane fuel cell environment. *Thin Solid Films* **2010**, *518*, 6598–6603. [[CrossRef](#)]
33. Park, Y.C.; Lee, S.H.; Kim, S.K.; Lim, S.; Jung, D.; Park, K.B.; Choi, S.Y.; Kim, J.H.; Peck, D.H. Corrosion properties and cell performance of CrN/Cr-coated stainless steel 316L as a metal bipolar plate for a direct methanol fuel cell. *Electrochim. Acta* **2011**, *56*, 7602–7609. [[CrossRef](#)]
34. Taneichi, D.; Haneda, R.; Aramaki, K. A novel modification of an alkanethiol self-assembled monolayer with alkylisocyanates to prepare protective films against copper corrosion. *Corros. Sci.* **2001**, *43*, 1589–1600. [[CrossRef](#)]
35. Björnkvist, L.; Olefjord, I. The electrochemistry of chromium in acidic chloride solutions: Anodic dissolution and passivation. *Corros. Sci.* **1991**, *32*, 231–242. [[CrossRef](#)]
36. Inturi, R.B.; Szklarska-Smialowska, Z. Localized corrosion of nanocrystalline 304 type stainless steel films. *Corrosion* **1992**, *48*, 398–403. [[CrossRef](#)]
37. Wang, L.; Nam, K.S.; Kwon, S.C. Effect of plasma nitriding of electroplated chromium coatings on the corrosion protection C45 mild steel. *Surf. Coat. Technol.* **2007**, *202*, 203–207. [[CrossRef](#)]
38. Wang, L.; Nam, K.S.; Kwon, S.C. Transmission electron microscopy study of plasma nitriding of electroplated chromium coating. *Appl. Surf. Sci.* **2003**, *207*, 372–377. [[CrossRef](#)]
39. Hamm, D.; Olsson, C.O.A.; Landolt, D. Effect of chromium content and sweep rate on passive film growth on iron–chromium alloys studied by EQCM and XPS. *Corros. Sci.* **2002**, *44*, 1009–1025. [[CrossRef](#)]



© 2018 by the authors. Licensee MDPI, Basel, Switzerland. This article is an open access article distributed under the terms and conditions of the Creative Commons Attribution (CC BY) license (<http://creativecommons.org/licenses/by/4.0/>).